Optimal cut in minimum spanning trees for 3-D cell nuclei segmentation

A. Abreu*†¶, F.-X.Frenois†, S. Valitutti ‡, P. Brousset §, P. Denèfle¶, B. Naegel * and C. Wemmert*
*ICube, University of Strasbourg, France
†Department of Pathology, Institut Universitaire du Cancer-Oncopôle, Toulouse, France
‡INSERM U.1043, Centre de Physiopathologie de Toulouse-Purpan, France
§INSERM U.1037, Centre de Recherches en Cancérologie de Toulouse, France
¶Institut Roche, Boulogne-Billancourt, France

***Abstract*—In biology and pathology immunofluorescence microscopy approaches are leading techniques for deciphering of the molecular mechanisms of cell activation and disease progression. Although several commercial softwares for image analysis are presently in the market, available solutions do not allow a totally non subjective image analysis. There is therefore strong need for new methods that could allow a completely non-subjective image analysis procedure including for thresholding and for choice of the objects of interest. To address this need, we describe a fully automatic segmentation of cell nuclei in 3-D confocal immunofluorescence images. The method merges segments of the image to fit with a nuclei model learned by a trained random forest classifier. The merging procedure explores efficiently the fusion configurations space of an over-segmented image by using minimum spanning trees of its region adjacency graph.**

I. Introduction

Functional imaging with multiplexed immunofluorescence together with whole-slide confocal microscopy enables biologists and pathologists to detect the expression of various proteins of interest in entire tissue samples, together with the ability to explore their spatial configurations and relationships in 3-D.

These technologies appear to be especially useful in cancer research for the study of the interactions between tumor cells and cells of the immune system, such as Cytotoxic T Cells (CTL). They have the potential to help to discover new tumor signatures and to precise the classification of patients in order to predict and enhance their responses to treatment and to provide a personal medication adapted to each well-defined kind of tumor. However, if tumor characterization at the cellular and molecular levels can lead to functional validation of targets for therapy and preclinical evaluation of treatment response, the major drawbacks are that whole-slide 3-D microscopy imaging techniques generate large sets of data to be analyzed. This leads to an increasing number of objects to extract from the images, that tend to be more and more complex [1], [2], [3].

Tools for interactive segmentation have already been developed in order to help biologists to quantify objects and events in both 3-D and 2-D images [4], [5], [6]. But interactive segmentation remains a time-consuming and tedious task, that is not well suited for image stacks containing hundreds or thousands of cells. Interactive tools are also likely to increase inter/intra-observer variability and induce subjectivity in the segmentation process.

Obviously, when a larger number of cells is to be analyzed in a study, fully automated methods are faster and less subjective. On the other hand, human brain integrates so much context information, prior knowledge and deductions based on image data that automatic segmentation tends to be much lower than visual analysis by an expert and automatic segmentation of digital pathology images remains a difficult challenge [7].

Particularly in fluorescent biological images, one recurrent and well studied task is the segmentation of cell nuclei which can be considered as the first step to complete multiplex image analysis. Commonly, one channel of the image is given by the fluorescence of dihydrochloride (DAPI), which labels DNA and reveals nuclei. Due to heterogeneities in DNA density, DAPI channel presents a signal with high intra/inter-nuclei intensity variability. Additionally, nuclei are usually in the form of dense clusters that have to be separated (see Fig. 4).

Fully automated methods for 3-D-nuclei segmentation have been extensively explored in the literature [8], [9], [10], [11], [12], [13], [14], [15], [16], [17], [18], [19]. Some of these approaches rely on implicit methods [15], [16] that are very sensitive to initialization and require high computation cost. However, they stand as excellent refinement methods since they define a smooth constrained model of the surface of a nucleus.

Other algorithms propose to separate clustered nuclei by finding and matching concavity points around the contours of clusters [17], [18], [19]. Though, contours of clusters are usually noisy and complex decision rules have to be created to eliminate outliers and find best matching points. Moreover, curvature is only computed on 2-D images and transcriptions of these methods to 3-D spaces imply to use an arbitrary slice of confocal images.

Most approaches are based on the marker-controlled watershed segmentation framework [8], [9], [10], [11], [12], [13], [14], where potential centers of nuclei are used as sources for the watershed procedure. The method is known to produce over-segmented images because of imperfect markers i.e. nuclei centers detection. To overcome the issue, models of nuclei are designed [9], [10], [11], [12] and a procedure of merging, ruled by models fitting, is used to find best fusion configurations. Exploring fusion configurations is a hard combinatorial problem and design of nuclei models as well as decision rules are treated as a heuristic.

978-1-5090-4011-7/17/$31.00

Our work is closely related to the latter category of algorithms. Nevertheless, we propose to reduce the exploration of fusion configurations with an original algorithm based on minimum spanning trees structures [20] and base our fusion decision rule on the predictions of a random forest classifier [21].

II. Methods

We propose a method for three-dimensional cell nuclei segmentation. We address the segmentation task as a region merging problem. After over-segmenting the volume with a classical watershed-based procedure, regions are used as nodes of a graph from which a minimum spanning tree is extracted. Then, the segmentation is performed by splitting iteratively the structure into sub-graphs that are most likely to be nuclei, where probability of being a nuclei is the prediction of a trained random forest classifier.

A. Initial segmentation

Initializing segmentation procedures with the result of a seeded watershed is a relatively common practice in 3-D cell nuclei segmentation [8], [9], [10], [11], [12], [13], [14]. The objective of this first step is to obtain labeled regions from the input grayscale image f. A binary mask is first generated from the input image by the use of Otsu's threshold value [22]. The Euclidian distance map is then computed from the mask and gives a grayscale image that is used as propagation map for the watershed. Seeds locations for the watershed, defined as potential centers of nuclei, are then computed as the local maxima of the distance map.
Though, based on nuclei's radius prior knowledge and a physical interpretation of the distance map, we can reduce the number of seeds. Let r_{min} be the radius of the smallest nuclei we aim to detect. Considering values in the distance map as physical distances, only peaks higher than r_{min} will be used as seeds.
Moreover, as we want to prevent different nuclei from being clustered into the same labeled region after segmentation, minimal distance between two detected seeds must be set to a value that does not exceed $2 \times r_{min}$.

B. Modeling and classification

1) Modeling: Model-based approaches are increasingly popular in the field of automatic histopathological analysis and have been successfully implemented to perform several tasks of detection and segmentation of cell nuclei both in 2-D and 3-D images [23], [24], [13]. They rely on a mathematical definition of a nucleus that gathers prior knowledge about shape and intensity in order to make segmentation procedures less sensitive to noisy and corrupted data. Let R_i be a labeled region of f. The modeling part of the workflow takes R_i and its corresponding values in f as an input and returns a feature vector x_i that is a descriptor of the region. Intensity and 3-D shape description of a nucleus remains a difficult task and, as in many related works [10], [11], we decided to use a vector of hand designed features described below:

- **Volume** is a simple count of all pixels in R_i;
- **Conv** is a measure of convexity, computed as the ratio between the volume of the convex hull and the actual volume of R_i;
- **Dx**, **Dy** and **Dz** are the dimensions of the bounding box of R_i;
- **Comp** is a measure of compacity, computed as the ratio between the volume of the bounding box and the actual volume of the R_i;
- **Front** is the fraction of points of the contour of R_i that actually separate R_i from other labeled regions of the image (background of the image is not a labeled region).
- **Var** is the variance of grayscale intensity in R_i.

2) Classification: Feature vectors can then be used to classify regions provided by the segmentation in two classes, *nuclei* and *non-nuclei*, or even define more subclasses for heterogeneous nuclei populations analysis [14]. Classical workflows propose to perform dimensionality reduction and linear discriminant analysis [25] to transform data into a new lower-dimensional space where separability between defined classes is as large as possible. Then, decision rules can be set by achieving cluster analysis on training data set.

However, considering our feature vector, no assumption can be made about data separability. In addition, labeling semi-automatically nuclei data is a time-consuming and onerous process that usually leads to small data sets with potentially high number of mislabeled data. Hence we choose the random forest classifier, since it is non-linear, has a low computation cost and relies on average decision of multiple independent predictors which decrease the risk of overfitting and make the classifier more resilient to outliers [21]. The number of trees n used for prediction is a parameter of the classifier that is set by the user. Large numbers provide better results and increase precision and reliability of class membership probabilities. Let $P_{i,c}$ be the probability of R_i to be a member of class C and denote by n_c the trees that actually predict R_i to be in class C. $P_{i,c}$ is calculated as the proportion of n_c among all trees in the forest.

To train the classifier, a relatively large number of hand-labeled shapes has to be produced. We extracted shapes from several confocal images by using part of the workflow described in next sections. Detail of the manual labeling procedure is given in section III-B.

C. Optimal cut of minimum spanning trees

To handle fusion combinations, we first turn regions from initial segmentation into a region adjacency graph (RAG) data structure [26] in which each region is a node and any touching pair of regions is an edge. RAG has then to be divided into subgraphs that best fit with our nuclei models. Unfortunately, maximizing nuclei model fitting over the RAG is not a suitable optimization problem for the Graph Cut framework [27]. Several algorithms have been proposed to address the problem with an original bottom-up hierarchical approach [10], [11], [14]. Briefly, they first assign to each node n of the RAG its optimal fusion configuration. Let SG be the whole set of possible fusion configurations containing node n

and s be an element of SG. Optimal element $s^*(n)$ of SG and its corresponding class affiliation $c^*(n)$ is defined as below.

$$(s^*(n), c^*(n)) = argmax_{(s,c)}(P_{s,c}) \quad (1)$$

Then, for each node n, $s^*(n)$ is kept i.e. fusion is actually done if condition below is satisfied.

$$\forall m \in s^*(n), \quad (2)$$
$$P_{s^*(n),c^*(n)} \geq P_{s^*(m),c^*(m)} \quad (3)$$

We propose a slightly different top-down approach that does not explore all fusion configurations for each node and can potentially bring an improvement in computation cost.
Our main idea is to turn RAG into a weighted graph and use the weights to compute a minimum spanning tree (MST) with Kruskal's algorithm [20]. The MST is a set of edges that connects all RAG regions together without creating any cycle. Kruskal's algorithm generates a spanning tree that minimize the total edge weight in the graph. Many choices are possible for the weighting function and each of them can lead to slightly different MST. Efficiency of our approach relies on two desirable properties of the MST (see Fig. 1): first, any node that is a fragment of a nucleus must be linked to, at least, one fragment of that same nucleus. Second, a node that is a fragment of a nucleus cannot be linked to more than one fragment from any other nucleus. Considering these properties and our application, the distance between centroids of nodes gave the best rate of receivable MST.

MST is an acyclic graph, which makes it a very convenient data structure to explore fusions of regions. By removing an edge of an MST, the tree is automatically splitted in two disconnected sub-trees. Let ST be the set that contains the MST itself as well as the sub-trees obtainable by removing exactly one edge in the MST. Then, given the MST and a classifier, optimal cut is the procedure that returns the sub-tree t^* defined by:

$$t^* = argmax_{(t \in ST)}(P_{t,nuclei}) \quad (4)$$

A simplified version of the optimal cut procedure is given in Fig. 3. The ability of the procedure to return the MST itself covers the case of isolated nuclei that does not have to be splitted: the MST itself is t^*. The procedure also returns the $residual$ tree obtained by removing nodes and edges of t^* from the MST. Complete segmentation of the MST is performed by applying the optimal cut procedure on successive $residual$ trees. For the purpose of segmentation, classifier only has to predict whether an object is a nucleus or not, but another procedure using the same random forest classifier can then be used for nuclei classification.

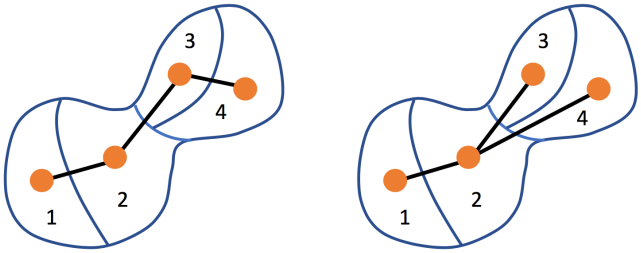

Fig. 1. Left: MST is admissible since removing edge (2, 3) results in a correct separation of clustered nuclei. Right: MST is non-admissible since edge removal cannot lead to a correct separation.

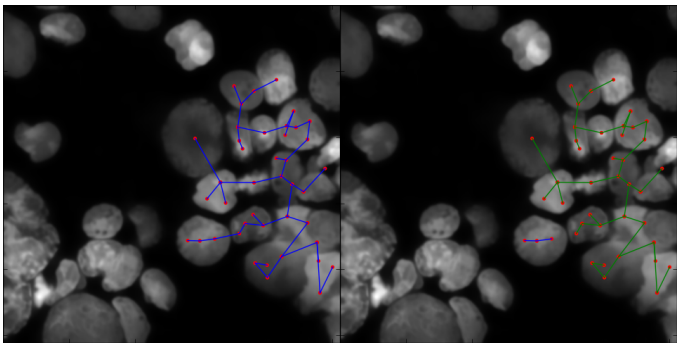

Fig. 2. Left: example of MST. Right: the first optimal cut of the MST.

procedure OPTIMAL CUT($MST, image, classifier$)
  $t^* \leftarrow MST$
  $residual \leftarrow None$
  $p^* \leftarrow P_{MST,nucleus}(image, classifier)$
  $ST \leftarrow getST(MST)$
  for t in ST **do**
    if $P_{MST,nucleus}(image, classifier) > p^*$ **then**
      $p^* \leftarrow P_{t,nucleus}(image, classifier)$
      $t^* \leftarrow t$
      $residual \leftarrow MST \setminus \{t\}$
    end if
  end for
  return $t^*, residual$
end procedure

Fig. 3. Optimal cut procedure

III. EXPERIMENTS

A. Image acquisition

Images of cytospins containing a mix of CTLs and melanoma cells were acquired with a Panoramic Confocal whole-slide digital microscope (3DHISTECH, Hungary) which relies on spinning grid and structured illumination technologies. This scanner is equipped with a PCO.edge 5.5 peltier-cooled sCMOS sensor, with a 40X NA 1.20 C-Apochromat water immersion objective, and uses a Lumencor Spectra X light engine with 6 independent illumination channels ranging from 374 to 762 nm.
The images are composed of 5 independent channels using optical filters whose bandwidths correspond to the peaks of excitation and emission spectra of 5 different dyes labelling specific biologically relevant objects. Our developments are done on a specific spectral channel coming from digital images acquired in 3-D (31 sections 400 nm spaced each : total volume = 12,4μm) using an optical filter whose bandwidths correspond to the peaks of excitation and emission spectra of DAPI which labels nuclei. Discretization parameters are given

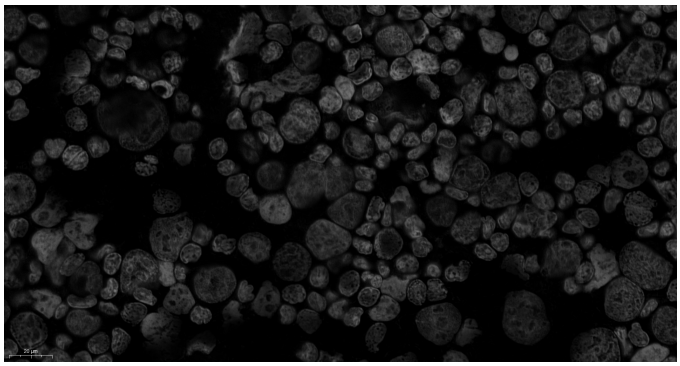

Fig. 4. Extract of a section of a panoramic confocal whole-slide image (size: 1920 x 1018 pixels, resolution: 162 nm per pixel).

TABLE I. IMAGE GEOMETRY PARAMETERS

Optical section	1.43μm
Z-spacing	0.4μm
X-resolution	0.1625μm
Y-resolution	0.1625μm

TABLE II. DATA SETS POPULATIONS

Data sets	Nuclei	Unacceptable
Total	379	808
Training	141	359
Testing	238	449

in Table I. Initially, image channel dimensions in pixels are $19200 \times 20736 \times 31$. For convenience, entire volume is divided in several smaller ($500 \times 500 \times 31$) volumes that are finally upsampled to $500 \times 500 \times 120$ matrices in order to get isotropic voxels (see TABLE I).

B. Training and testing

We used a sample of 30 of the previously defined sub-volumes as a data set. From that data set, 369 MST were automatically extracted to be manually segmented and labeled by the use of a Graphical User Interface (GUI). The interface superimpose a representation of the tree on a 2-D projection of the image. The user has to select a configuration of adjacent nodes and assign a class to its selection (see Fig. 5). We choose to limit the experiment to a simple classification problem with 2 classes, keeping classification of heterogeneous nuclei population for a future work: shapes are labeled "nuclei" or "unacceptable". Populations of manually extracted shapes are summarized in Table II. To validate the classification model, we used the misclassification rate of a thousand of random forest classifiers on our testing data set. Classifiers all have 200 estimators, are randomly initialized and trained on the 500 shapes of our training data set. Average misclassification rate over all the classifiers on the testing data set is 5.3%.

C. Segmentation evaluation

Independently from the training set of 30 images, 7 sub-volumes were manually segmented with the GUI in order to confront expert segmentation with our automatic method. Segmentation "by hand" ended up with 86 detected and segmented nuclei.

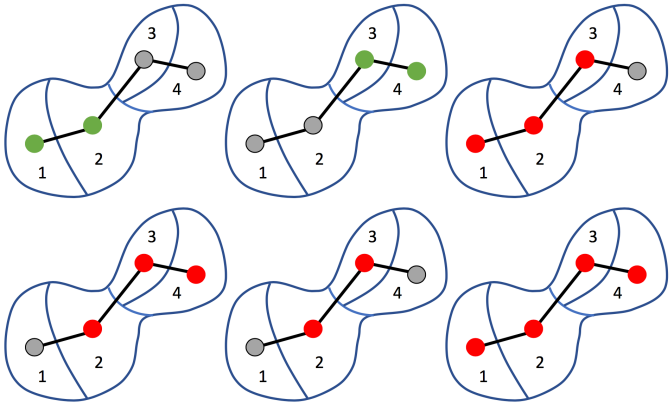

Fig. 5. Examples of manual segmentation and labeling. Green dots are configurations of MST's nodes that must be labeled as nuclei. Red dots are configurations of MST's nodes that must be labeled as unacceptable shapes.

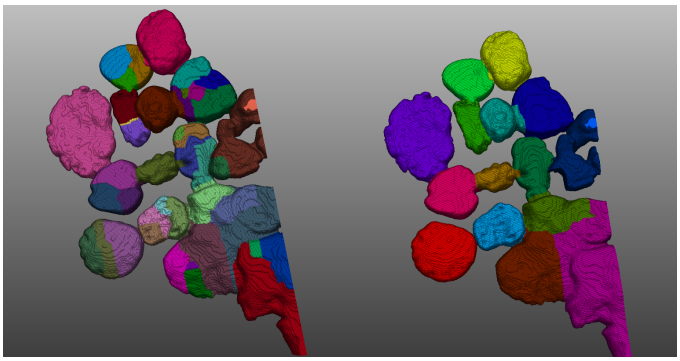

Fig. 6. Left: Initial over-segmentation. Right: Refined segmentation with optimal cut of the spanning tree.

For automatic segmentation, we used a $tolerance$ parameter of 0.5 for the optimal cut procedure i.e. a region R_i will not appear in the segmented image if $P_{i,nucleus} < 0.5$. In these conditions, our method detected and segmented 83 nuclei. Each automatically segmented nucleus appears to be in the set of manually segmented ones. Though the method missed 3 nuclei, detected and segmented objects seem to be reliable.

Further testing has to be done with a larger set of images, acquired from different biological experiments and image acquisition settings or devices, in order to test robustness of the described method.

IV. DISCUSSION AND CONCLUSION

We proposed a segmentation method of cells nuclei in 3-D immunofluorescence images. The method is part of the numerous approaches that seek best fusion configurations in a set of image fragments to fit nuclei models. We described an original method, based on minimum spanning trees of a region adjacency graph, to address the combinatorial problem of fusion configurations exploration and we proposed to replace heuristic and Bayesian region-ranking rules by the use of a powerful classifier.

However, current development remains a preliminary work. From a machine-learning point of view, data sets we used are relatively small and cannot be representative of data

variability since they are extracted from only two different images acquired with the same device. Thus, performances of the classifier are not intensively tested and its ability to classify heterogeneous populations of cells still has to be proven.

Finally, as in many similar approaches, a tremendous improvement would be to free ourselves from designing nuclei models "by hand" and obtain features with less subjectivity with solutions like stacked autoencoders or others deep learning approaches.

ACKNOWLEDGMENT

The authors would like to thank 3DHISTECH for their material support. Arnaud Abreu is supported by a CIFRE fellowship founded in part by National Association for Research and Technology (ANRT) on the behalf of the French Ministry of Higher Education and Research, and in part by ROCHE Institute.

REFERENCES

[1] M. Faroudi, C. Utzny, M. Salio, V. Cerundolo, M. Guiraud, S. Müller, and S. Valitutti, "Lytic versus stimulatory synapse in cytotoxic T lymphocyte/target cell interaction: manifestation of a dual activation threshold," *Proceedings of the National Academy of Sciences*, vol. 100, no. 24, pp. 14 145–14 150, 2003.

[2] D. Depoil, R. Zaru, M. Guiraud, A. Chauveau, J. Harriague, G. Bismuth, C. Utzny, S. Müller, and S. Valitutti, "Immunological synapses are versatile structures enabling selective T cell polarization," *Immunity*, vol. 22, no. 2, pp. 185–194, 2005.

[3] A. Wiedemann, D. Depoil, M. Faroudi, and S. Valitutti, "Cytotoxic T lymphocytes kill multiple targets simultaneously via spatiotemporal uncoupling of lytic and stimulatory synapses," *Proceedings of the National Academy of Sciences*, vol. 103, no. 29, pp. 10 985–10 990, 2006.

[4] M. Czader, A. Liljeborg, G. Auer, and A. Porwit, "Confocal 3-dimensional DNA image cytometry in thick tissue sections," *Cytometry Part A*, vol. 25, no. 3, pp. 246–253, 1996.

[5] S. J. Lockett, D. Sudar, C. T. Thompson, D. Pinkel, and J. W. Gray, "Efficient, interactive, and three-dimensional segmentation of cell nuclei in thick tissue sections," *Cytometry*, vol. 31, no. 4, pp. 275–286, 1998.

[6] K. Rodenacker, M. Aubele, P. Hutzler, and P. Umesh Adiga, "Groping for quantitative digital 3-D image analysis: an approach to quantitative fluorescence in situ hybridization in thick tissue sections of prostate carcinoma," *Analytical Cellular Pathology*, vol. 15, no. 1, pp. 19–29, 1997.

[7] H. Irshad, A. Veillard, L. Roux, and D. Racoceanu, "Methods for nuclei detection, segmentation, and classification in digital histopathology: a review current status and future potential," *IEEE Reviews in Biomedical Engineering*, vol. 7, pp. 97–114, 2014.

[8] C. Ortiz De Solrzano, E. Garcia Rodriguez, A. Jones, D. Pinkel, J. W. Gray, D. Sudar, and S. J. Lockett, "Segmentation of confocal microscope images of cell nuclei in thick tissue sections," *Journal of Microscopy*, vol. 193, no. 3, pp. 212–226, 1999.

[9] M. K. Chawla, G. Lin, K. Olson, A. Vazdarjanova, S. N. Burke, B. L. McNaughton, P. F. Worley, J. F. Guzowski, B. Roysam, and C. A. Barnes, "3D-catFISH: a system for automated quantitative three-dimensional compartmental analysis of temporal gene transcription activity imaged by fluorescence in situ hybridization," *Journal of neuroscience methods*, vol. 139, no. 1, pp. 13–24, 2004.

[10] G. Lin, U. Adiga, K. Olson, J. F. Guzowski, C. A. Barnes, and B. Roysam, "A hybrid 3D watershed algorithm incorporating gradient cues and object models for automatic segmentation of nuclei in confocal image stacks," *Cytometry Part A*, vol. 56, no. 1, pp. 23–36, 2003.

[11] G. Lin, M. K. Chawla, K. Olson, J. F. Guzowski, C. A. Barnes, and B. Roysam, "Hierarchical, model-based merging of multiple fragments for improved three-dimensional segmentation of nuclei," *Cytometry Part A*, vol. 63, no. 1, pp. 20–33, 2005.

[12] P. U. Adiga and B. Chaudhuri, "An efficient method based on watershed and rule-based merging for segmentation of 3-D histopathological images," *Pattern Recognition*, vol. 34, no. 7, pp. 1449–1458, 2001.

[13] C. Wählby, I.-M. SINTORN, F. Erlandsson, G. Borgefors, and E. Bengtsson, "Combining intensity, edge and shape information for 2D and 3D segmentation of cell nuclei in tissue sections," *Journal of Microscopy*, vol. 215, no. 1, pp. 67–76, 2004.

[14] G. Lin, M. K. Chawla, K. Olson, C. A. Barnes, J. F. Guzowski, C. Bjornsson, W. Shain, and B. Roysam, "A multimodel approach to simultaneous segmentation and classification of heterogeneous populations of cell nuclei in 3D confocal microscope images," *Cytometry Part A*, vol. 71, no. 9, pp. 724–736, 2007.

[15] A. Dufour, V. Shinin, S. Tajbakhsh, N. Guillén-Aghion, J.-C. Olivo-Marin, and C. Zimmer, "Segmenting and tracking fluorescent cells in dynamic 3-d microscopy with coupled active surfaces," *IEEE Trans. Image Process.*, vol. 14, no. 9, pp. 1396–1410, 2005.

[16] A. Sarti, C. O. De Solorzano, S. Lockett, and R. Malladi, "A geometric model for 3-D confocal image analysis," *IEEE Trans. Bio-Med. Eng.*, vol. 47, no. 12, pp. 1600–1609, 2000.

[17] J. A. Beliën, H. A. van Ginkel, P. Tekola, L. S. Ploeger, N. M. Poulin, J. Baak, and P. J. van Diest, "Confocal DNA cytometry: A contour-based segmentation algorithm for automated three-dimensional image segmentation," *Cytometry Part A*, vol. 49, no. 1, pp. 12–21, 2002.

[18] J. Qi, "Dense nuclei segmentation based on graph cut and convexity-concavity analysis," *Journal of Microscopy*, vol. 253, no. 1, pp. 42–53, 2014.

[19] Q. Wen, H. Chang, and B. Parvin, "A Delaunay triangulation approach for segmenting clumps of nuclei," in *Biomedical Imaging: From Nano to Macro, 2009. ISBI'09. IEEE International Symposium on*. IEEE, Conference Proceedings, pp. 9–12.

[20] J. B. Kruskal, "On the shortest spanning subtree of a graph and the traveling salesman problem," *Proceedings of the American Mathematical society*, vol. 7, no. 1, pp. 48–50, 1956.

[21] L. Breiman, "Random forests," *Machine Learning*, vol. 45, no. 1, pp. 5–32, 2001. [Online]. Available: http://dx.doi.org/10.1023/A:1010933404324

[22] X. Du and S. Dua, "Segmentation of fluorescence microscopy cell images using unsupervised mining," *Open Medical Informatics Journal*, vol. 4, pp. 41–49, 2010.

[23] M. Alilou, V. Kovalev, and V. Taimouri, "Segmentation of cell nuclei in heterogeneous microscopy images: A reshapable templates approach," *Computerized Medical Imaging and Graphics*, vol. 37, no. 7, pp. 488–499, 2013.

[24] X. Descombes, "Multiple objects detection in biological images using a marked point process framework," *Methods*, 2016.

[25] R. O. Duda, P. E. Hart, and D. G. Stork, *Pattern classification*. John Wiley & Sons, 2012.

[26] M. Sonka, V. Hlavac, and R. Boyle, *Image processing, analysis, and machine vision*. Cengage Learning, 2014.

[27] V. Kolmogorov and R. Zabin, "What energy functions can be minimized via graph cuts?" *IEEE Trans. Pattern Anal. Mach. Intell.*, vol. 26, no. 2, pp. 147–159, 2004.